

Helical magnetic ordering studied in single-crystalline GdBe₁₃

Hiroyuki Hidaka¹,* Kota Mizuuchi, Eikai Hayasaka, Tatsuya Yanagisawa¹, Jun Ohara, and Hiroshi Amitsuka
 Graduate School of Science, Hokkaido University, Sapporo, Hokkaido 060-0810, Japan



(Received 3 June 2020; accepted 20 October 2020; published 6 November 2020)

The beryllide GdBe₁₃ with the NaZn₁₃-type face-centered-cubic structure has been known to undergo a proper helical-magnet ordering from experimental studies using polycrystalline samples. In the present study, we carried out electrical resistivity, specific heat, and magnetization measurements of single-crystalline GdBe₁₃ in order to investigate a mechanism of its helical ordering. These measurements reveal that the present compound is a metallic system exhibiting the magnetic ordering of local Gd³⁺ moments at $T_N = 24.8$ K accompanied with strong magnetic fluctuations extending to temperatures well above T_N . Furthermore, we constructed a magnetic field–temperature (B – T) phase diagram for $B \parallel [001]$. It consists of a multidomain state, which is composed of magnetic structures with B applied parallel and perpendicular to the helical plane, in the lower-magnetic-field region below ~ 0.45 T and a possible single-domain conical one in the higher-field region in the ordering state. The helical structure of GdBe₁₃ characterized by an incommensurate ordering vector \mathbf{q}_0 of (0, 0, 0.285) is discussed on the basis of a competition of Heisenberg exchange interactions between the Gd³⁺ moments assuming an one-dimensional layer crystal. The sequential change in the exchange interactions determined by a mean-field (MF) calculation can be essentially understood by the Ruderman-Kittel-Kasuya-Yosida interaction via anisotropic Fermi surfaces, whereas the orientation of the magnetic moments will be determined by the dipole-dipole interaction. On the other hand, the MF theory predicts a much smaller critical field B_c than the experimentally obtained one. To discuss the deviation of B_c from the MF calculation, we show a possibility of a fluctuation-induced first-order transition.

DOI: [10.1103/PhysRevB.102.174408](https://doi.org/10.1103/PhysRevB.102.174408)

I. INTRODUCTION

Helical magnets have been attracted much attention as a possible host compound for the emergence of peculiar spin textures, such as a magnetic skyrmion [1,2] and a chiral soliton [3,4]. Previous observations of the skyrmions have mostly been made in noncentrosymmetric systems with the Dzyaloshinsky–Moriya (DM) interaction in d -electron systems [1]. Very recently, the formation of skyrmions has been reported even for centrosymmetric systems with and without geometrical frustrations in several Gd-based compounds [5–7]. The role of the geometrical frustrations and the inversion symmetry breaking in the formation of skyrmions is still being discussed. To deepen understanding, the skyrmion formation mechanism, further investigations of detailed crystallographic, electronic, and magnetic properties in a typical helical magnet would be essential.

It is known that the beryllides MBe₁₃ (M = rare earths and actinides) also undergo the helical-magnetic ordering formed by well-localized f magnetic moments, mainly in heavy-rare-earth systems [8,9], although there is no report on the formation of the skyrmion thus far. They crystallize in the NaZn₁₃-type face-centered-cubic (FCC) structure with the space group $Fm\bar{3}c$ (No. 226, O_h^8) [8,10], where the M ions can be regarded as forming a simple cubic. Since the crystal structure holds the inversion symmetry, the DM interaction

is absent in the present system (however, there is no inversion symmetry at the M ion site with the site symmetry O). Because of these rather simple features, the MBe₁₃ system should be one of the most suitable materials to study the fundamental mechanism of the helical-magnetic ordering.

In the present study, we focus our attention on GdBe₁₃, which exhibits the helical-magnetic ordering at the highest ordering temperature T_N of 26 K in the MBe₁₃ compounds [8]. In principle, a trivalent Gd ion has no orbital angular momentum L ($4f^7$: $S = 7/2$, $L = 0$, and $J = 7/2$), so that experimental studies on GdBe₁₃ will provide fundamental insights into the helical ordering in the MBe₁₃ systems except for magnetocrystalline anisotropy associated with L . Here, S , L , and J are the total-spin, total-orbital, and total-angular momenta, respectively. Neutron diffraction measurements on powder sample revealed that the helical structure of GdBe₁₃ is the proper one with an incommensurate propagation vector \mathbf{q}_0 of (0, 0, 0.285) [11]. From previous magnetization (M) measurements using polycrystalline samples, a Curie–Weiss (CW) temperature θ_{CW} and a critical field of the helical ordering B_c were estimated to be +25 K and 7 T, respectively [8,12]. However, B_c is estimated to be about 1 T from the mean-field (MF) calculation using the reported T_N and θ_{CW} , which is far from the experimentally obtained value. The cause of this discrepancy remains unclear, but it might be attributed to some effect that cannot be explained in the MF theory, such as magnetic fluctuations. In order to solve this problem and reveal the detailed mechanism of the helical ordering for GdBe₁₃, further experimental studies using single crystals, which have

*hidaka@phys.sci.hokudai.ac.jp

not been done so far except for our recent M measurement using an as-grown single crystal [13], are needed.

The present paper reports the results of electrical resistivity (ρ), specific heat (C), and M measurements for single crystals of GdBe_{13} in temperatures of down to 2 K in magnetic fields of up to 7 T. The experimental results and a constructed magnetic phase diagram are presented in Sec. III. In addition, we discuss the mechanism of the helical-magnetic ordering in GdBe_{13} in Sec. IV: model for the helical ordering in Sec. IV A, MF calculation of the critical field in Sec. IV B, possibility of a fluctuation-induced first-order transition in Sec. IV C, and magnetic anisotropy originating in dipole interactions in Sec. IV D.

II. EXPERIMENT

Single crystals of GdBe_{13} were grown by the Al-flux method. The constituent materials (Gd with 99.9% purity and Be with 99.9% purity) and Al with 99.99% purity were placed in an alumina crucible at an atomic ratio of 1:13:35 and sealed in a quartz tube filled with Ar gas of ~ 150 mmHg. The sealed tube was kept at 1050 °C for 3 days and then cooled at a rate of 2 °C/h. The Al flux was spun off in a centrifuge and then removed by NaOH solution. The obtained single crystals were annealed for 2 weeks at 700 °C. The typical size of the grown sample is about $1 \times 1 \times 1$ mm³.

The powder x-ray diffraction (XRD) measurement was performed with a commercial powder x-ray diffractometer (SmartLab, Rigaku) using Cu $K\alpha_1$ and $K\alpha_2$ radiation in the angle range of $10^\circ < 2\theta < 120^\circ$ at room temperature. The as-grown samples of GdBe_{13} were ground into fine powder in the ethyl alcohol. The obtained XRD pattern can be explained by the NaZn_{13} -type cubic structure. We do not observe any peaks associated with impurity phases in the experimental accuracy, although the M measurements using the annealed single crystals revealed the presence of a tiny amount of magnetic impurities, mainly on the sample surface, as described in Appendix. A lattice constant of GdBe_{13} was obtained to be $a = 10.2804(1)$ Å, which is in good agreement with the previously reported value of $a = 10.273$ Å by Bucher *et al.* [8] and $a = 10.280(2)$ Å by Borsa and Olcese [14].

Electrical-resistivity ρ measurements were performed by a conventional four-probe method in the temperature range of 1.3–300 K with a hand-made ⁴He refrigerator using two single-crystalline samples assigned as 1 (as-grown) and 2 (annealed). The electrical current j was applied along the cubic [001] direction. The specific-heat C measurements were performed using sample 3 (annealed) by a thermal-relaxation method in the magnetic-field range of 0–7 T and in the temperature range of 2–300 K with a Physical Property Measurement System (PPMS, Quantum Design, Inc.). The DC magnetization measurements were performed using sample 2 (annealed) in the magnetic fields up to 7 T and in the temperature range from 2 to 350 K by a Magnetic Property Measurement System (MPMS, Quantum Design, Inc.). In both the M and C measurements, the magnetic field B was applied along the [001] direction. The samples of 1–3 were taken from the same sample batch, and sample surfaces of sample 2 were polished after annealing to eliminate an influence of the magnetic impurities as possible.

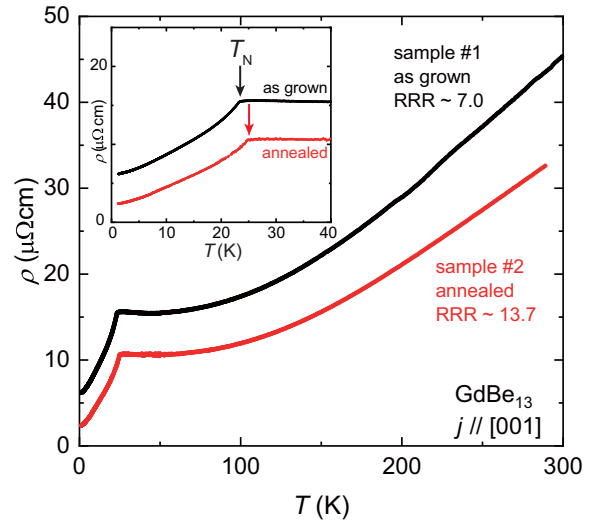


FIG. 1. Temperature dependence of the electrical resistivity $\rho(T)$ of GdBe_{13} for the as-grown and annealed single-crystalline samples. The inset shows the enlarged view below 40 K. The arrows indicate the transition temperature T_N .

III. EXPERIMENTAL RESULTS

A. Electrical resistivity

Figure 1 shows the temperature dependence of the electrical resistivity $\rho(T)$ of GdBe_{13} for the as-grown sample 1 and annealed sample 2. The sample 2 was polished on its surfaces to remove the magnetic impurities. The $\rho(T)$ measurements reveal that the residual resistivity ratio (RRR) increases from 7.0 to 13.7, and the residual resistivity decreases from 6.2 to 2.4 $\mu\Omega\text{cm}$ by the sample annealing. For the polished sample 2 after annealing, the $\rho(T)$ curve exhibits simple metallic behavior. On the other hand, for the unpolished sample 1, ρ increases slightly below ~ 45 K, which may come from the Kondo effect due to contamination of magnetic impurities.

The inset of Fig. 1 displays that enlarged view of $\rho(T)$ below 40 K. Both the $\rho(T)$ curves show a kink anomaly due to the helical ordering at T_N . The kink at T_N for the annealed sample is more distinct and the value of T_N ($=24.8$ K) becomes higher than that for the as-grown sample ($=23.3$ K). Similar annealing effect has also been observed in SmBe_{13} [17]. On the other hand, the obtained T_N for the annealed sample is lower than that of ~ 26 K obtained from the previous M and C measurements for polycrystalline samples [8,12].

B. Specific heat

Figure 2 shows the temperature dependence of the specific heat divided by the temperature $C(T)/T$ for the annealed sample 3 of GdBe_{13} . In this figure, $C(T)/T$ of LaBe_{13} is also displayed as a reference for the phonon contribution in GdBe_{13} [15]. The data of LaBe_{13} obeys a Debye T^3 law below ~ 10 K, where the Sommerfeld coefficient γ and the Debye temperature θ_D have been estimated to be ~ 9.1 mJ K⁻² mol⁻¹ and ~ 950 K, respectively [15]. In addition to the Debye phonon, the MBe_{13} systems have a low-energy Einstein-like phonon mode with its characteristic temperature θ_E of ~ 160 K [15–17], which can be observed as a broad hump at around

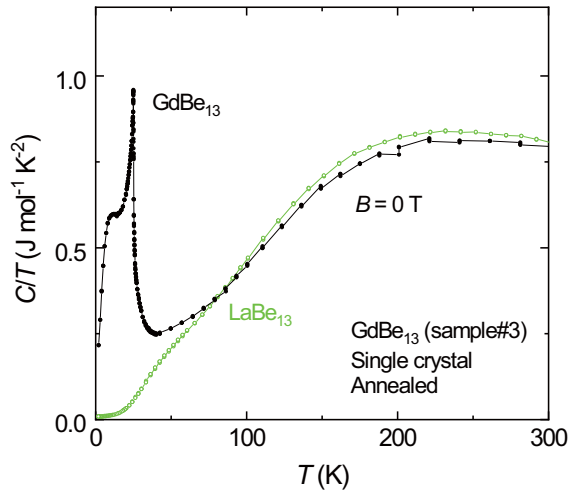


FIG. 2. Temperature dependence of C/T for GdBe_{13} (closed circles) and LaBe_{13} (open circles) [15] below 300 K at zero field.

40 K in $C(T)/T$. The $C(T)/T$ curve of GdBe_{13} also exhibits a hump-like structure near 40 K, suggesting that the present compound also has the low-energy Einstein phonon with $\theta_E \sim 160$ K. The value of C/T for GdBe_{13} is slightly smaller than that for LaBe_{13} above ~ 80 K, which may be due to the difference in the Debye phonon contribution.

To estimate the magnetic contribution to the specific heat C_{mag} of GdBe_{13} , we subtract $C(T)$ of LaBe_{13} from that of GdBe_{13} . Figure 3 shows the temperature dependence of C_{mag}/T at zero magnetic field. This curve exhibits a sharp peak at $T_N = 25.0$ K, which is very close to that determined in the present ρ measurements for the annealed sample. The height and shape in $C_{\text{mag}}(T)/T$ at T_N appear to suggest a first-order phase transition, as discussed in Sec. IV. In addition, a shoulder structure can be seen in $C_{\text{mag}}(T)/T$ near 8 K. Such a shoulder below a magnetic transition temperature has often been observed in Gd^{3+} and Eu^{2+} compounds with $J = 7/2$ [18–20]. It is known that the shoulder appears at $\sim T_N/4$, which is attributed to splitting of the $J = 7/2$ multiplet due to an internal field [21]. The shoulder for GdBe_{13} would be also understood by the same explanation.

Temperature dependence of magnetic entropy S_{mag} , which was obtained by integrating $C_{\text{mag}}(T)/T$ with respect to T from 2 K, is also displayed in Fig. 3. The obtained S_{mag} saturates near the theoretical high- T limit value of $R\ln 8 = 17.3 \text{ J mol}^{-1} \text{ K}^{-1}$ for $J = 7/2$ above ~ 70 K, indicating well-localized $4f^7$ state of the Gd^{3+} ions. It is characteristic that S_{mag} starts to decrease from a temperature well above T_N with decreasing temperature, and then it reaches $0.76R\ln 8$ at T_N . The relatively large reduction of S_{mag} from the full entropy suggests the presence of strong fluctuations of the localized magnetic moments in the wide temperature region above T_N . Similar large reduction of S_{mag} ($= 1/2R\ln 8$) has also been observed in a helical magnet EuPtSi with Eu^{2+} for $J = 7/2$, where the first-order phase transition occurs at T_N [22].

The $C_{\text{mag}}(T)/T$ data below 40 K at several fields up to 7 T for $B \parallel [001]$ are shown in Fig. 4. T_N shifts to the lower temperature side and the peak anomaly at T_N becomes broader as B increases. At $B = 7$ T, no anomaly is observed in

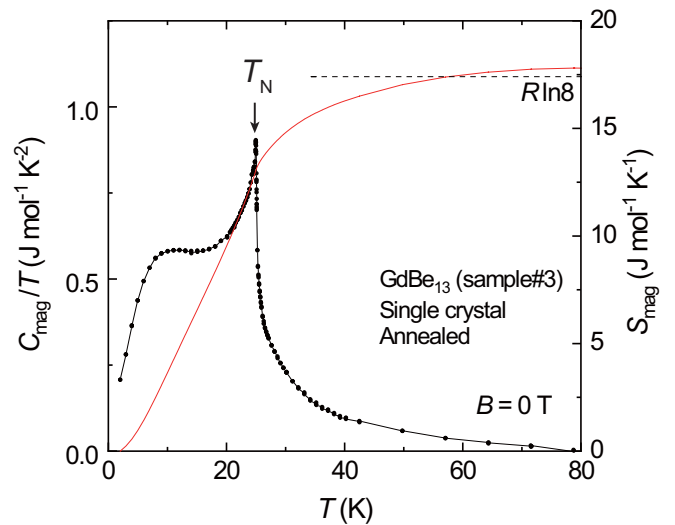


FIG. 3. Temperature dependence of C_{mag}/T (left axis) and S_{mag} (right axis) in GdBe_{13} at zero magnetic field. The horizontal dashed line represents the full entropy value of $R\ln 8$ for $J = 7/2$.

$C_{\text{mag}}(T)/T$ down to 2 K except for a broad maximum around 10 K, suggesting that B_c is between 6 and 7 T. The broad maximum near 10 K can be explained by the splitting of the $J = 7/2$ multiplet. The solid curve in this figure represents the calculation result of the Schottky specific heat assuming the splitting of the $J = 7/2$ octet, where we adopted the level splitting between each state to be 25 K.

C. Magnetic susceptibility and magnetization curve

Figure 5 shows the temperature dependence of the inverse magnetic susceptibility $\chi^{-1}(T) [= B/M(T)]$ of GdBe_{13} at $B = 5$ T for the annealed sample 2. Although the measured sample was polished on its surface after annealing to remove the impurity, the remained magnetic impurities of $\sim 0.03\%$, which

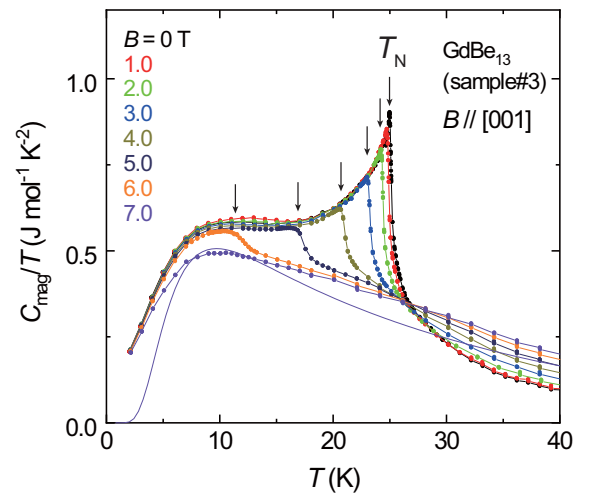


FIG. 4. Temperature dependence of C_{mag}/T for GdBe_{13} at several magnetic fields up to 7 T. The magnetic field is applied along the $[001]$ axis. The solid curve represents the calculation result of the Schottky specific heat assuming the splitting of the $J = 7/2$ octet.

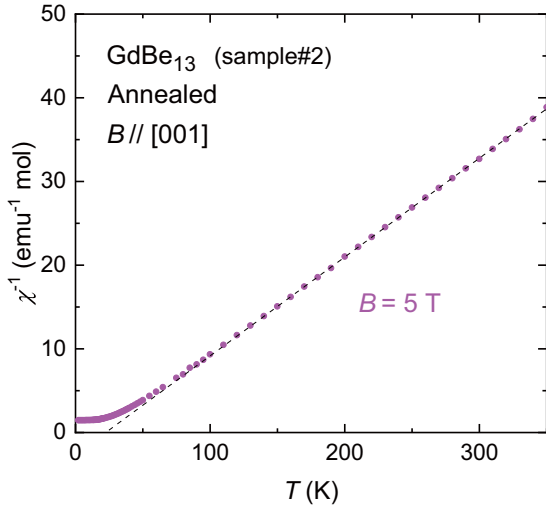


FIG. 5. Temperature dependence of the inverse magnetic susceptibility $\chi^{-1}(T)$ [$= B/M(T)$] of GdBe_{13} for the annealed sample 2 at $B = 5$ T applied along [001]. The dashed line represents a CW fit in the temperature range between 150 and 350 K.

should be a ferromagnet GdAl_2 with the Curie temperature T_C of 175 K [23], is evidenced by a ferromagnetic anomaly visible in $\chi^{-1}(T)$ at a small field and a hysteretic behavior in magnetization process near zero field (see Appendix). The obtained $\chi^{-1}(T)$ at 5 T reveals linear temperature dependence in high temperature range, where the influence of the magnetic impurities appears to be negligible. We performed a CW fit, described by $\chi^{-1}(T) = 3k_B(T - \theta_{CW}) / (N_A \mu_B^2 \mu_{\text{eff}}^2)$, on the obtained data between 150 and 350 K. Here, k_B is the Boltzmann constant, θ_{CW} a CW temperature, N_A Avogadro's number, μ_B the Bohr magneton, and μ_{eff} the effective magnetic moment. From this fit, θ_{CW} and μ_{eff} were obtained to be $+22.4(5)$ K and $8.23(1) \mu_B/\text{Gd}$, respectively. The μ_{eff} value determined is slightly larger than that expected in a free Gd^{3+} ion and that reported in the previous M measurements using polycrystalline samples [8], both of which are $7.94 \mu_B/\text{Gd}$. The difference in μ_{eff} between the polycrystal and the single crystal might be due to the presence of defects of the Gd ions in the present single crystal. On the other hand, the positive θ_{CW} , whose absolute value is close to T_N , indicates the predominant ferromagnetic (FM) interaction between the Gd^{3+} moments. These features concerning θ_{CW} are common in the rare-earth based MBe_{13} compounds showing the helical ordering [8,17].

Figure 6(a) shows the temperature dependence of the magnetic susceptibility $\chi(T)$ [$= M(T)/B$] for GdBe_{13} at $B = 0.1$ T below 50 K. The open and closed symbols represent the data upon zero-field-cooling (ZFC) and field-cooling (FC) processes, respectively. A cusp anomaly can be observed at $T_N = 24.8$ K in $\chi(T)$, which is in good agreement with that obtained from the present ρ and C measurements. Below T_N , a difference between the ZFC and FC processes can be observed in $\chi(T)$ at this magnetic field, suggesting a magnetic multidomain state in the ordering phase. In addition to the cusp anomaly, the $\chi(T)$ curve exhibits an inflection at $T^* \sim 28$ K. Here, T^* was determined by the temperature at which $d\chi(T)/dT$ takes the minimum, as shown in the inset of Fig. 6(a). Such an inflection just above T_N has been also found

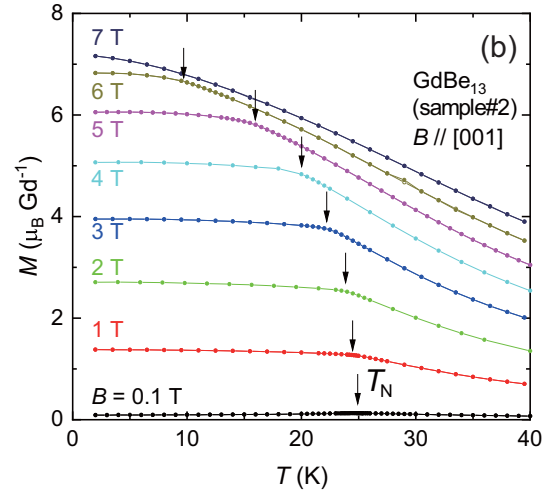
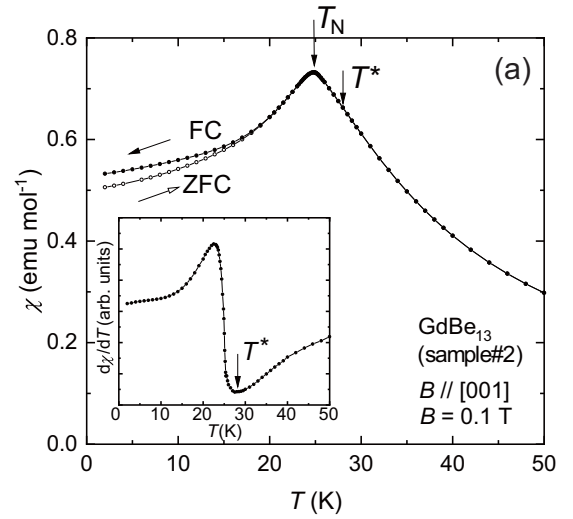


FIG. 6. (a) Temperature dependence of the magnetic susceptibility $\chi(T)$ [$= M(T)/B$] for GdBe_{13} below 50 K at $B = 0.1$ T applied along [001]. The open and closed symbols represent the data upon ZFC and FC processes, respectively. The inset shows $d\chi/dT$ as a function of T at 0.1 T. (b) Temperature dependence of the magnetization $M(T)$ at several fields up to 7 T for $B \parallel [001]$.

in helical magnets MnSi and EuPtSi , where development of strongly interacting magnetic fluctuations below T^* has been pointed out [24,25].

Figure 6(b) displays the temperature dependence of the magnetization $M(T)$ at several fields up to 7 T for $B \parallel [001]$. The $M(T)$ curves above 1 T exhibit a kink anomaly at T_N , not the cusp anomaly, below where the data shows no difference between the ZFC and FC processes. Here, T_N above 1 T were determined by the temperature where d^2M/dT^2 takes the local minimum. These results suggest a change from the magnetic multidomain state to a different one with a single-domain structure between 0.1 and 1 T. The kink anomaly at T_N decreases with increasing B , and it disappears in the data at 7 T. The field dependence of T_N obtained from the present M measurements is in good agreement with that obtained from the present C measurements.

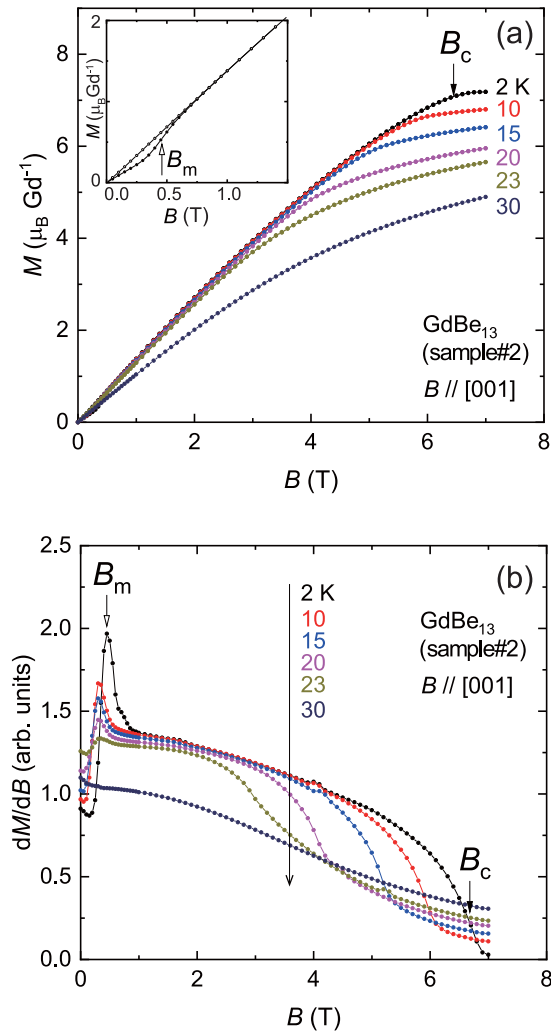


FIG. 7. (a) Magnetization process up to 7 T of GdBe_{13} at several temperatures below 30 K. B was applied along the [001] direction. The inset shows the data at 2 K in the field region below 1.5 T. The closed and open symbols indicate the increasing- and decreasing-field processes, respectively. (b) The respective derivative dM/dB versus temperature upon the increasing-field process. In both the figures, the open and closed arrows represent B_m and B_c , respectively.

Figure 7(a) shows the magnetization process $M(B)$ up to 7 T of GdBe_{13} for the annealed sample 2, measured at various temperatures between 2 and 30 K. The magnetic field was applied along the [001] direction. At the lowest temperature of 2 K, M increases in the upper convexity with increasing B , and then reaches the saturation value M_s of $\sim 7.2 \mu_B/\text{Gd}$ above $B_c \sim 6.7$ T, which is close to the Gd^{3+} free ion moment of $7 \mu_B/\text{Gd}$. Here, we determined B_c by a peak of $-d^2M/dB^2$. Note that the convex curve is not consistent with the helical structure for which a linear dependence is expected. The value of B_c decreases with increasing temperature, and the saturating behavior becomes indistinct. Above T_N , M increases monotonously as B increases in whole the B region.

The $M(B)$ curves for GdBe_{13} at 2 K upon increasing- and decreasing-field processes in the low field region below 1.5 T are shown in the inset of Fig. 7(a). One can see a metamagnetic-like behavior at $B_m \sim 0.45$ T on

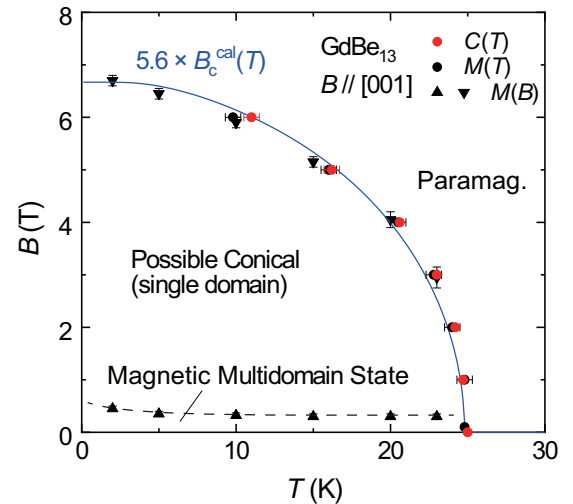


FIG. 8. Magnetic field-temperature (B - T) phase diagram of GdBe_{13} for $B \parallel [001]$, constructed from the M and C measurements using the annealed single crystals. The dashed curve is guide to the eye, while the solid curve indicates $5.6 \times B_c^{\text{cal}}(T)$ obtained by the MF calculation (see text).

the increasing-field process. Similar metamagnetic behavior has also been found in an isostructural helical magnet HoBe_{13} , where the magnetic structure above the metamagnetic field has been revealed to be a conical one [26]. The metamagnetic-like transition in GdBe_{13} is also considered to correspond to the transition from the magnetic multidomain state to the conical one. On the other hand, the $M(B)$ curve upon the decreasing-field process shows almost linear-field dependence. The difference between the increasing- and decreasing-field processes can be interpreted as follows. Once the possible conical structure with the single domain becomes stable in the high-field region, the magnetic structure could not turn back to the multidomain state, which would consist of magnetic structures with B applied parallel and perpendicular to the helical plane, even below B_m . If the magnetic structure below B_m after applying high-magnetic fields is a single-domain helical with its helical plane perpendicular to B , which cannot be distinguished from the conical, the linear-field dependence in $M(B)$ for decreasing field can be explained. Similar magnetization process has been also found in MnSi when B is applied along the [111] direction, where similar magnetic multidomain state has been discussed [27]. With increasing temperature, the B_m anomaly becomes indistinct and B_m slightly shifts to the lower-field side; however, the anomaly persists up to 23 K. Here, B_m is determined by the peak of dM/dB in each $M(B)$ curve upon the increasing-field process [see Fig. 7(b)]. It is commented that the present result concerning B_m is consistent with that reported for polycrystalline GdBe_{13} by Roy and Stewart, where the anomaly was observed accompanied with hysteresis at $B_m \sim 0.3$ T [28].

D. Magnetic phase diagram

The magnetic field-temperature (B - T) phase diagram of GdBe_{13} for $B \parallel [001]$, constructed from the present $C(T)$, $M(T)$, and $M(B)$ measurements, is shown in Fig. 8. The experimentally obtained $B_c(T)$ corresponds to the result of the

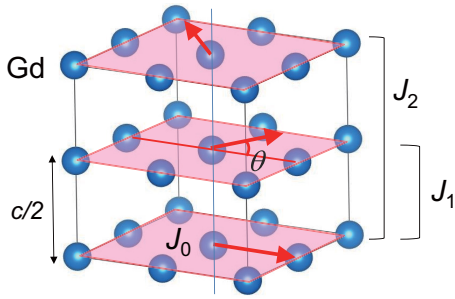


FIG. 9. Generic helical structure of GdBe_{13} . The Heisenberg exchange interactions J_0 , J_1 , and J_2 are indicated in this figure. θ is the turn angle of the magnetic moment between adjacent layers. The distance between adjacent layers corresponds to a half of the lattice constant of the FCC lattice.

MF calculation multiplied by 5.6 (the blue solid curve), as discussed in the next section. This magnetic phase diagram consists of two regions in the ordering state: the multidomain state composed of the magnetic structures with B applied parallel and perpendicular to the helical plane below B_m and the possible single-domain conical state above B_m . This rather simple phase diagram of GdBe_{13} may originate from the absence of the single-ion anisotropy of the Gd^{3+} ions. It is known that other isostructural MBe_{13} systems showing the helical ordering have a B - T phase diagram consisting of more than three regions in the ordered state [17,26]. For example, Dervenagas *et al.* suggested that the appearance of the third magnetic phase at higher fields in HoBe_{13} , which corresponds to the canted-conical magnetic structure, is provided by the single-ion anisotropy on the Ho^{3+} ion [26].

IV. DISCUSSION

A. Model for the helical ordering

The helical ordering of the rare-earth based MBe_{13} has been explained by a competition between intralayer and interlayer Heisenberg exchange interactions for an one-dimensional layer crystal, as shown in Fig. 9 [11,29]. In this model, J_0 is the sum of all Heisenberg exchange interactions of a representative spin to all other spins in the same spin layer perpendicular to the helix axis, J_1 is the sum of all interactions in an adjacent layer along the helix axis, and J_2 is the sum of all interactions in a second-nearest layer. The total exchange energy can be expressed as [30]

$$E(\theta) = -NJ^2(J_0 + 2J_1\cos\theta + 2J_2\cos2\theta). \quad (1)$$

Here, N is total number of spins, J is the total angular momentum, and θ is the turn angle between magnetic moments in adjacent planes. Furthermore, within the MF theory, T_N , θ_{CW} , and the turn angle in the ordered state θ_0 are related to J_0 , J_1 , and J_2 through [30]:

$$T_N = \frac{2J(J+1)}{3k_B}(J_0 + 2J_1\cos\theta_0 + 2J_2\cos2\theta_0), \quad (2)$$

$$\theta_{\text{CW}} = \frac{2J(J+1)}{3k_B}(J_0 + 2J_1 + 2J_2), \quad (3)$$

$$\cos\theta_0 = -\frac{J_1}{4J_2}. \quad (4)$$

These three exchange constants J_0 , J_1 , and J_2 can be obtained by solving Eqs. (2)–(4).

For GdBe_{13} with $J = 7/2$, we can get the exchange interactions from the following experimental results: $T_N = 24.8$ K, $\theta_{\text{CW}} = 22.4$ K, and $\mathbf{q}_0 = 0.285c^*$ [11]. θ_0 is given by $2\pi\mathbf{q}_0 \cdot c/2$. Here, we define the c axis as the helical axis of the magnetic structure in a cubic crystal for convenience. The obtained exchange interactions are

$$J_0 = +0.91 \text{ K}, \quad J_1 = +1.02 \text{ K}, \quad J_2 = -0.41 \text{ K}.$$

Note that similar calculation has been performed in the previous report by Vigneron *et al.*,

$$J_0 = +1.36 \text{ K}, \quad J_1 = +0.85 \text{ K}, \quad J_2 = -0.34 \text{ K},$$

where they used $T_N = 27$ K and $\theta_{\text{CW}} = 25$ K for the polycrystalline sample [31]. These obtained parameters are essentially consistent with the one-dimensional layer model mentioned above, where FM layers ($J_0 > 0$) stack along the direction of \mathbf{q}_0 , and a frustration between the FM layers ($J_1 > 0$ and $J_2 < 0$) is present.

The dominant exchange interaction in GdBe_{13} is not direct one but indirect one of the Ruderman-Kittel-Kasuya-Yosida (RKKY) type, since the distance between Gd ions is greater than 5 Å. The RKKY interaction commonly plays a dominant role for the magnetic ordering in a metallic system with localized f electrons, where the intersite exchange coupling between the f moments is mediated by itinerant conduction electrons [32]. The RKKY-type exchange interaction J_{RKKY} is given by

$$J_{\text{RKKY}} \propto D(E_F)J_{\text{cf}}F(2k_F r), \quad (5)$$

where $D(E_F)$ is the density of state at the Fermi energy, J_{cf} the exchange interaction between the f moments and the conduction electron spin, k_F the Fermi wave vector, r the distance between interacting sites, and $F(x)$ the RKKY oscillation function ($= [-x\cos(x) + \sin(x)]/x^4$). The RKKY interaction is usually expected to cause a damped oscillation of the exchange interactions against r with changing its sign due to $F(x)$. The sequential change in the exchange interactions of GdBe_{13} can be understood by the RKKY oscillation except for $J_0 < J_1$ determined in the present study. These results suggest that the helical structure of GdBe_{13} is based on the delicate balance of the exchange interactions attributed to the high symmetry of the Gd-ion lattice, although the experimental problems still remain, such as the difficulty of determining θ_{CW} and the difference in T_N and θ_{CW} between the polycrystal and the single crystal. More precise M measurements on single crystals with higher quality are required in order to discuss the values of the exchange interactions more strictly.

In addition, a direction of \mathbf{q}_0 should also originate from the RKKY interaction. Though the RKKY interaction is originally assumed to be isotropic with a spherical Fermi surface (FS), an actual band structure is usually more complicated in a material. The band calculation for LaBe_{13} without 4f electrons revealed the presence of relatively large FSs along the [001] direction (at X point) and the [111] direction (at L point) but absent along the [110] direction (at K point) [33,34]. It is considered that the band structure for GdBe_{13} is similar to that for LaBe_{13} , because the 4f electrons of GdBe_{13} are well localized. Thus the FS being present at the X point

would determine the direction of \mathbf{q}_0 for the helical ordering in GdBe₁₃.

B. Mean-field calculation of the critical field

Next, we estimate the critical field B_c of GdBe₁₃ on the basis of the MF theory, when magnetic field is applied perpendicular to the zero-field ordered moments. The following MF calculation is expected to be applicable in general antiferromagnets with identical crystallographically equivalent spins interacting by Heisenberg exchange; in other word, we do not assume the one-dimensional layer model in this section. The MF prediction for B_c at absolute zero is given by [30]

$$B_c^{\text{cal}}(T=0) = \frac{3k_B}{gJ\mu_B(J+1)}(T_N - \theta_{\text{CW}}). \quad (6)$$

On the other hand, the magnitude of thermal average of J is given by $|\langle J \rangle| = J\sigma$. Here, σ is given by numerically solving the following self-consistency equation:

$$\sigma = B_J \left[\frac{3J}{J+1} \frac{T_N}{T} \sigma \right] \quad (7)$$

where $B_J(x)$ is the Brillouin function. The product of $B_c^{\text{cal}}(T=0)$ and $\sigma(T)$ provides the temperature variation of the critical field $B_c^{\text{cal}}(T)$. Using $T_N = 24.8$ K and $\theta_{\text{CW}} = +22.4$ K obtained from the $M(T)$ measurements, $B_c^{\text{cal}}(T=0)$ is estimated to be ~ 1.19 T, which is approximately 1/5.6 of the experimentally obtained B_c of 6.7 T at $T = 2$ K. On the other hand, the $B_c^{\text{cal}}(T)$ curve can be reproduced well the experimental one by multiplied by 5.6, as displayed in Fig. 8. The deviation of B_c from the MF calculation has been already pointed out in the previous measurements using polycrystals [11,12]. Note that similar MF calculation for $B_c(T)$ has been succeeded in explaining quantitatively the experimental data in a helical-magnet EuCo_{2-y}As₂ with Eu²⁺ ions [35]. Since the quantitative difference between experimentally obtained B_c and the calculated B_c^{cal} cannot be explained by the uncertainty in the measured quantity of T_N and θ_{CW} , it will be necessary to consider some additional effect beyond the MF theory.

C. Possibility of fluctuation-induced first-order transition

One possible explanation for the discrepancy between B_c and B_c^{cal} is suppression of T_N due to a fluctuation-induced first-order transition (FIFOT). In general, the helical-magnetic transition is expected to be of a second order on the MF theory, while it has been predicted theoretically that interactions between the helical-magnetic fluctuations give rise to important corrections driving the first-order phase transition. The emergence of such a FIFOT has been experimentally reported in several helical magnets, such as MnSi and EuPtSi [22,24,25,36]. Bak *et al.* proposed an antiferromagnetic (AFM) system described by a number of components of order parameter $n > 4$ as a possible material showing the FIFOT [37]. Furthermore, theoretical calculation by the Monte Carlo technique has predicted that the actual transition temperature is suppressed much below the MF transition temperature by the FIFOT [38]. GdBe₁₃ is a strong candidate for exhibiting the FIFOT, since the number of n is counted to be 12 by the

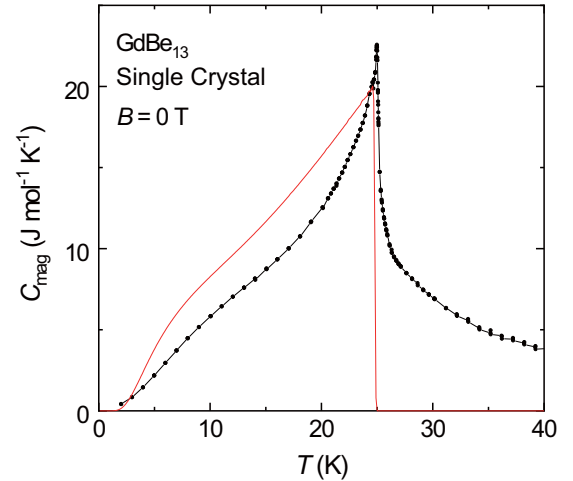


FIG. 10. Magnetic contribution to the specific heat C_{mag} as a function of temperature for GdBe₁₃ at $B = 0$ T. The red line represents the data obtained from the MF calculation based on the results in the present $\chi(T)$ measurements.

product of the star of \mathbf{q}_0 consisting of the six vectors and two independent direction of the magnetization for each \mathbf{q}_0 .

One of the experimental evidence for the FIFOT in GdBe₁₃ would be the sharp peak at T_N in $C_{\text{mag}}(T)$. Figure 10 shows the experimentally obtained $C_{\text{mag}}(T)$ curve of GdBe₁₃ with $T_N = 25.0$ K at $B = 0$ T and the MF calculation result based on $T_N = 24.8$ K and $\theta_{\text{CW}} = 22.4$ K obtained from the present $\chi(T)$ data. The larger maximum value and the sharper peak at T_N in the experimental data suggest the first-order phase transition, although we can observe no thermal hysteresis in $C_{\text{mag}}(T)$ in the experimental accuracy. Note that the first-order nature of C_{mag} is more pronounced in the measurement using a polycrystalline sample, where the maximum value reaches about 30 J mol⁻¹ K⁻¹ [12]. In addition, the inflection at T^* in the $\chi(T)$ curve implies development of the interaction between the magnetic fluctuations below T^* , as observed in MnSi and EuPtSi [24,25]. If T_N of GdBe₁₃ is not suppressed by the strongly interacting fluctuations, the experimentally obtained B_c might correspond to B_c^{cal} .

D. Magnetic anisotropy originating in dipole interactions

Finally, we discuss how the orientation of the magnetic moments is determined in the ordered state of GdBe₁₃. Though the largest contribution to the magnetic anisotropy usually comes from single-ion magnetic anisotropy in rare-earth based systems, Gd³⁺ ion should be hardly influenced by the single-ion anisotropy attributed to L . Instead, it is known that the dipole-dipole interaction plays an important role in the magnetic anisotropy of Gd compounds. In many Gd³⁺-based AFM compounds, the orientation of the magnetic moments can be explained by a straightforward numerical method considering the dipole interaction, when \mathbf{q}_0 is known [39]. To predict the orientation of the magnetic moments of GdBe₁₃, we performed similar numerical calculation based on the dipole-dipole interaction between Gd ions. Here, we assumed a simple cubic lattice consisting of the Gd ions as a primitive cell, where its lattice constant and $\mathbf{q}_0 = (0, 0, 0.285)$

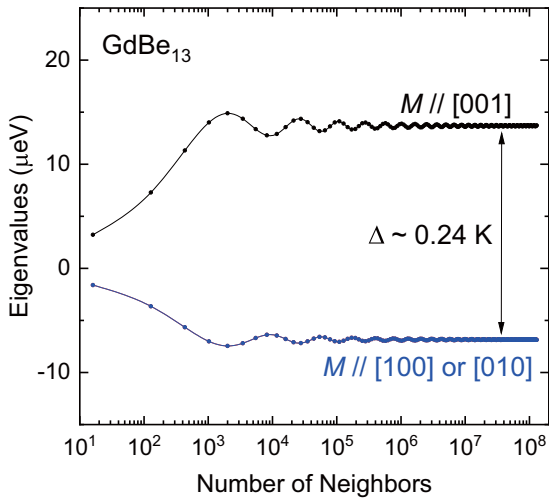


FIG. 11. Convergence behavior of the eigenvalues of the Fourier transform of the dipole interaction tensor $J_{\alpha\beta}(\mathbf{q}_0)$ in GdBe_{13} with respect to number of neighbor ions. The definition of $J_{\alpha\beta}(\mathbf{q}_0)$ is referred to Ref. [39].

become half of the original ones. A detailed description of the analytical method is given in Ref. [40].

The obtained convergence of the eigenvalues of the Fourier transform of the dipole interaction tensor $J_{\alpha\beta}(\mathbf{q}_0)$ with respect to the number of neighbor ions at absolute zero is shown in Fig. 11. Note that our definition of sign of the eigenvalues is opposite to that in Ref. [39]. The larger and smaller eigenvalues correspond to states that the magnetic moments point to the [001] direction and the [100] or [010] direction, respectively. These results reveal that the magnetic moments prefer to point to the direction perpendicular to \mathbf{q}_0 . They also indicate that there is no magnetic anisotropy in the (001) plane, which is favorable to a proper helical structure. Thus the present numerical calculation based on the dipole interaction can reproduce the orientation of the magnetic moments in the helical state for GdBe_{13} . In addition, one can estimate an ordering temperature originating from the dipole interaction T_N^{dipole} . It is given by [40]

$$T_N^{\text{dipole}} = \Delta J(J+1)/3. \quad (8)$$

Here, Δ is the difference between the eigenvalues, which is a measure of the dipolar anisotropy. For $\Delta \sim 0.24$ K in GdBe_{13} , T_N^{dipole} is estimated to be ~ 1.26 K, which is much lower than T_N of 24.8 K obtained experimentally. This result means that the dipole interaction is not a driving force of the helical ordering for GdBe_{13} . On the other hand, a critical field of the ordering originating from the dipole interaction B_c^{dipole} can be estimated to be ~ 0.27 T from $k_B T_N^{\text{dipole}}/g_J J \mu_B$. This value of B_c^{dipole} is comparable to the experimentally obtained B_m . The magnetic anisotropy coming from the dipole interaction may play a key role in the change of the magnetic structure from the magnetic multidomain state to the single-domain conical one for GdBe_{13} .

V. SUMMARY

We have succeeded in growing single crystals of an incommensurate helical magnet GdBe_{13} by the Al-flux method and performed ρ , C and M measurements at magnetic fields up to 7 T for $B \parallel [001]$ using the grown single crystals. The ρ measurements indicate normal metallic behavior with a kink anomaly in $\rho(T)$ at $T_N = 24.8$ K. From the C and M measurements, we obtained the following features concerning the helical ordering for GdBe_{13} : (i) $4f^7$ electrons of Gd^{3+} ions are well localized, (ii) the obtained θ_{CW} of +22.5 K is positive and close to T_N , (iii) strong magnetic fluctuation persists up to temperatures far above T_N , and (iv) a critical field of the ordering state B_c is ~ 6.7 T. These are essentially consistent with those reported in the previous C and M measurements using polycrystalline samples [8,11,12]. In addition to them, we constructed a B - T phase diagram for $B \parallel [001]$, which indicates that a possible conical phase is present above $B_m \sim 0.45$ T in the ordering state.

We also discussed the incommensurate helical structure with $\mathbf{q}_0 = (0, 0, 0.285)$ in GdBe_{13} by a competition of the Heisenberg exchange interactions assuming an one-dimensional layer crystal, which has been proposed in the previous reports [11,29]. It is argued that the exchange interactions obtained from the MF calculation and the direction of \mathbf{q}_0 derive from the RKKY interaction via anisotropic Fermi surfaces. Furthermore, numerical calculation considering the dipole-dipole interaction reveals that the orientation of the magnetic moments can be explained by only the dipole interaction between the Gd^{3+} moments. These revealed features would provide useful insights not only into the common magnetism in the MBe_{13} systems, but also into the fundamental magnetism in other helical magnets. On the other hand, the problem that B_c predicted by the MF calculation is much smaller than the experimental value is still unsolved. As one possible answer, we proposed the possibility that a FIFOT takes place at T_N , and it plays a key role in the difference in B_c . To deepen our understanding of the magnetic property in the present system, further studies, such as investigation of the magnetic anisotropy and detailed annealing effects, are needed and now in progress.

ACKNOWLEDGMENTS

The authors are grateful to H. Harima for helpful comments on the band structure of the MBe_{13} system and to F. Kon and C. Tabata for great helps on the powder XRD measurements. The present research was supported by JSPS KAKENHI Grants No. JP20224015(S), No. JP25400346(C), No. JP26400342(C), No. JP17K05525(C), No. JP15H05882, No. JP15H05885(J-Physics), and No. JP20K03825. This study was also partly supported by Hokkaido University, Global Facility Center (GFC), Advanced Physical Property Open Unit (APPOU), funded by MEXT under Support Program for Implementation of New Equipment Sharing System Grants No. JPMXS0420100316, No. JPMXS0420100317, No. JPMXS0420100318, No. JPMXS0420100319, and No. JPMXS0420100320, and the Open Facility, GFC, Creative Research Institution, Hokkaido University for allowing us to

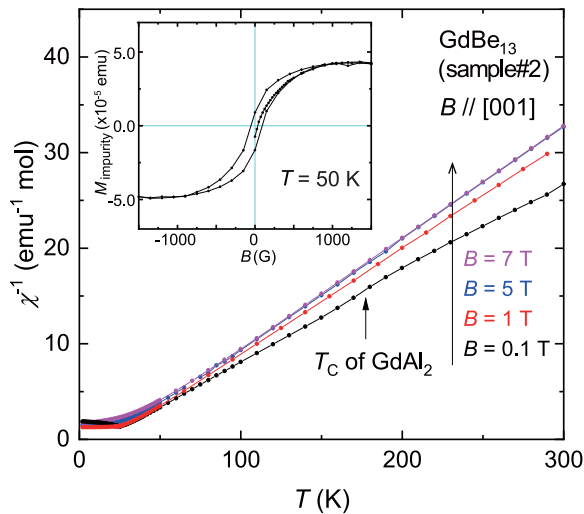


FIG. 12. Temperature dependence of the inverse magnetic susceptibility $\chi^{-1}(T)$ at $B = 0.1, 1, 5,$ and 7 T in GdBe_{13} for the annealed sample 2. B is applied along the $[001]$ direction. The closed arrow located at 175 K indicates T_C of GdAl_2 . The inset shows M_{impurity} vs magnetic field near zero field at 50 K. M_{impurity} was obtained by subtracting the paramagnetic component from M of the measured sample.

conduct the analysis of GdBe_{13} using SmartLab and providing insight and expertise that greatly assisted the research.

APPENDIX: CONTAINED MAGNETIC IMPURITY

The single crystals of GdBe_{13} grown by the Al-flux method in the present study contain the magnetic impurity, which should be a ferromagnet GdAl_2 with T_C of 175 K [23]. The $\chi^{-1}(T)$ curves at 0.1 and 1 T show a bend at around T_C of GdAl_2 , as can be seen in Fig. 12. The bend in $\chi^{-1}(T)$ at the low fields is more distinct for an unpolished sample after annealing (not shown). On the other hand, the data above 5 T show a linear temperature dependence, where the influence of the magnetic impurity becomes negligibly small. In addition, the amount of the FM impurity was estimated from a hysteretic behavior in the $M(B)$ curve below T_C of GdAl_2 . The inset of Fig. 12 shows the magnetization coming from the FM impurity ($\equiv M_{\text{impurity}}$) as a function of B at 50 K, which was obtained by subtracting a linear component corresponding to a paramagnetic state from the measured M . This plot reveals that the saturation value M_s of this $M(B)$ curve is $\sim 5 \times 10^{-5}$ emu. When we assume that all the M_s comes from the ordered moments of $7 \mu_B/\text{Gd}$ in GdAl_2 , the amount of the FM impurity can be estimated to be $\sim 0.03\%$ of the total sample.

- [1] N. Kanazawa, S. Seki, and Y. Tokura, *Adv. Mater.* **29**, 1603227 (2017).
- [2] S. Mühlbauer, B. Binz, F. Jonietz, C. Pfleiderer, A. Rosch, A. Neubauer, R. Georgii, and P. Böni, *Science* **323**, 915 (2009).
- [3] T. Matsumura, Y. Kita, K. Kubo, Y. Yoshikawa, S. Michimura, T. Inami, Y. Kousaka, K. Inoue, and S. Ohara, *J. Phys. Soc. Jpn.* **86**, 124702 (2017).
- [4] Y. Togawa, T. Koyama, K. Takayanagi, S. Mori, Y. Kousaka, J. Akimitsu, S. Nishihara, K. Inoue, A. S. Ovchinnikov, and J. Kishine, *Phys. Rev. Lett.* **108**, 107202 (2012).
- [5] T. Kurumaji, T. Nakajima, M. Hirschberger, A. Kikkawa, Y. Yamasaki, H. Sagayama, H. Nakao, Y. Taguchi, T. Arima, and Y. Tokura, *Science* **365**, 914 (2019).
- [6] M. Hirschberger, T. Nakajima, S. Gao, L. Peng, A. Kikkawa, T. Kurumaji, M. Kriener, Y. Yamasaki, H. Sagayama, H. Nakao, K. Ohishi, K. Kakurai, Y. Taguchi, X. Yu, T. Arima, and Y. Tokura, *Nat. Commun.* **10**, 5831 (2019).
- [7] N. D. Khanh, T. Nakajima, X. Z. Yu, S. Gao, K. Shibata, M. Hirschberger, Y. Yamasaki, H. Sagayama, H. Nakao, L. C. Peng, K. Nakajima, R. Takagi, T. Arima, Y. Tokura, and S. Seki, *Nat. Nanotechnol.* **15**, 444 (2020).
- [8] E. Bucher, J. P. Maita, G. W. Hull, R. C. Fulton, and A. S. Cooper, *Phys. Rev. B* **11**, 440 (1975).
- [9] F. Bourée-Vigneron, *Phys. Scr.* **44**, 27 (1991).
- [10] M. W. McElfresh, J. H. Hall, R. R. Ryan, J. L. Smith, and Z. Fisk, *Acta Cryst.* **C46**, 1579 (1990).
- [11] F. Vigneron, M. Bonnet, A. Herr, and J. Schweizer, *J. Phys. F: Met. Phys.* **12**, 223 (1982).
- [12] M. J. Besnus, G. L. F. Fraga, and D. Schmitt, *J. Alloys Compd.* **235**, 59 (1991).
- [13] H. Hidaka, K. Mizuuchi, T. Yanagisawa, and H. Amitsuka, *JPS Conf. Proc.* **30**, 011117 (2020).
- [14] F. Borsa and G. Olcese, *Phys. Status Solidi A* **17**, 631 (1973).
- [15] H. Hidaka, Y. Shimizu, S. Yamazaki, N. Miura, R. Nagata, C. Tabata, S. Mombetsu, T. Yanagisawa, and H. Amitsuka, *J. Phys. Soc. Jpn.* **86**, 023704 (2017).
- [16] H. Hidaka, R. Nagata, C. Tabata, Y. Shimizu, N. Miura, T. Yanagisawa, and H. Amitsuka, *Phys. Rev. Materials* **2**, 053603 (2018).
- [17] H. Hidaka, S. Yamazaki, Y. Shimizu, N. Miura, C. Tabata, T. Yanagisawa, and H. Amitsuka, *J. Phys. Soc. Jpn.* **86**, 074703 (2017).
- [18] M. Bouvier, P. Lethuillier, and D. Schmitt, *Phys. Rev. B* **43**, 13137 (1991).
- [19] S. Süllow, I. Prasad, M. C. Aronson, J. L. Sarrao, Z. Fisk, D. Hristova, A. H. Lacerda, M. F. Hundley, A. Vigliante, and D. Gibbs, *Phys. Rev. B* **57**, 5860 (1998).
- [20] H. Hidaka, Y. Ikeda, I. Kawasaki, T. Yanagisawa, and H. Amitsuka, *Physica B* **404**, 3005 (2009).
- [21] J. A. Blanco, D. Gignoux, and D. Schmitt, *Phys. Rev. B* **43**, 13145 (1991).
- [22] D. G. Franco, Y. Prots, C. Geibel, and S. Seiro, *Phys. Rev. B* **96**, 014401 (2017).
- [23] E. W. Lee and J. F. D. Montenegro, *J. Magn. Magn. Mater.* **22**, 282 (1981).
- [24] M. Janoschek, M. Garst, A. Bauer, P. Krautscheid, R. Georgii, P. Böni, and C. Pfleiderer, *Phys. Rev. B* **87**, 134407 (2013).
- [25] T. Sakakibara, S. Nakamura, S. Kittaka, M. Kakihana, M. Hedo, T. Nakama, and Y. Ōnuki, *J. Phys. Soc. Jpn.* **88**, 093701 (2019).

- [26] P. Dervenagas, P. Burllet, M. Bonnet, F. Bourdarot, A. Hiess, S. L. Bud'ko, P. C. Canfield, G. H. Lander, J. S. Kim, and G. R. Stewart, *Phys. Rev. B* **61**, 405 (2000).
- [27] V. N. Narozhnyi and V. N. Krasnorussky, *Phys. Rev. B* **91**, 134403 (2015).
- [28] S. B. Roy and G. R. Stewart, *J. Magn. Magn. Mater.* **99**, 235 (1991).
- [29] P. J. Becker, M. Bonnet, and F. Vigneron, *Mol. Cryst. Liq. Cryst.* **125**, 405 (1985).
- [30] T. Nagamiya, *Solid State Phys.* **20**, 305 (1967).
- [31] Since the definition of the exchange interaction is different between the present study and the previous study of Ref. [11], we recalculated the exchange interactions using the values of T_N and θ_{CW} for polycrystal in our definition.
- [32] S. J. Frisken and D. J. Miller, *Phys. Rev. Lett.* **57**, 2971 (1986).
- [33] K. Takegahara, H. Harima, and T. Kasuya, *J. Phys. F: Met. Phys.* **16**, 1691 (1986).
- [34] H. Harima (private communication).
- [35] N. S. Sangeetha, V. K. Anand, E. Cuervo-Reyes, V. Smetana, A.-V. Mudring, and D. C. Johnston, *Phys. Rev. B* **97**, 144403 (2018).
- [36] A. Bauer, M. Garst, and C. Pfleiderer, *Phys. Rev. Lett.* **110**, 177207 (2013).
- [37] P. Bak, S. Krinsky, and D. Mukamelg, *Phys. Rev. Lett.* **36**, 52 (1976).
- [38] O. G. Mouritsen, S. J. Knak Jensen, and P. Bak, *Phys. Rev. Lett.* **39**, 629 (1977).
- [39] M. Rotter, M. Loewenhaupt, M. Doerr, A. Lindbaum, H. Sassik, K. Ziebeck, and B. Beuneu, *Phys. Rev. B* **68**, 144418 (2003).
- [40] M. Rotter, M. Loewenhaupt, M. Doerr, A. Lindbaum, and H. Michor, *Phys. Rev. B* **64**, 014402 (2001).